Mitigation of defocusing by statics and near-surface velocity errors by interferometric least-squares migration

Mrinal Sinha and Gerard T. Schuster, King Abdullah University of Science and Technology*

SUMMARY

We propose an interferometric least-squares migration method that can significantly reduce migration artifacts due to statics and errors in the near-surface velocity model. We first choose a reference reflector whose topography is well known from the, e.g., well logs. Reflections from this reference layer are correlated with the traces associated with reflections from deeper interfaces to get crosscorrelograms. These crosscorrelograms are then migrated using interferometric least-squares migration (ILSM). In this way statics and velocity errors at the near surface are largely eliminated for the examples in our paper.

INTRODUCTION

The shallow velocity model may be erroneous, and can severely defocus the migration images at deeper depth. Conventional statics removal methods can be inadequate in removing statics from the data. These errors may arise due to complex overburden or low-velocity anomalies in the shallow subsurface.

Zhou et al. (2006) introduced the concept of interferometric migration to mitigate the defocusing due to the statics contained in the data. In this method they shifted the data by the traveltime of the picked reference reflections. This time-shift can also be automatically computed by cross-correlating the trace windowed around the reference reflection with the original trace. This procedure is carried out for all the traces and it nearly cancels out the phase associated with the common raypaths above the reference interface for small-offsets. It also has the merit of approximately redatuming the data to the reference interface.

One of the problems with this method is that the correlated traces can lead to artifacts in the migration image and the reference reflections must be carefully windowed. To mitigate the correlation artifacts in the final migration image, we extend the interferometric migration method of Zhou et al. (2006) to a least-squares inversion scheme where the final migration image is computed by minimizing an interferometric cross-correlation objective function. Here, the objective function is formed by zero-lag correlation of the recorded and simulated cross-correlograms.

This paper is organized into four sections. After the introduction, the second section describes the theory of interferometic least-squares migration. Numerical results on synthetic and field data are presented in the next section, and the conclusions are in the last section.

THEORY

Let the observed data in the frequency domain be denoted by $\tilde{D}(\mathbf{g}|\mathbf{s})$ and the predicted data be denoted by $D(\mathbf{g}|\mathbf{s})$ for a source at $\mathbf{s}$ and geophone at $\mathbf{g}$. Let $D(\mathbf{g}|\mathbf{s})_{ref}$ denote the trace that is windowed around a reference reflection event. To estimate the crosscorrelogram $\Phi(\mathbf{g}|\mathbf{s})$ the windowed reference reflections in the data are cross-correlated with the recorded traces as :

$$\Phi(\mathbf{g}|\mathbf{s}) = D(\mathbf{g}|\mathbf{s})D^{*}(\mathbf{g}|\mathbf{s})_{ref}. \tag{1}$$

Similarly, the observed crosscorrelogram $\tilde{\Phi}(\mathbf{g}|\mathbf{s})$ can be obtained by cross-correlation of recorded traces with the observed reference reflection traces. The goal is to find the reflectivity model which maximizes the normalized dot product of the observed and predicted crosscorrelograms. This can be written as (Routh et al. (2011); Zhang et al. (2013); Dutta et al. (2014)),

$$\varepsilon = -\sum_{\omega}\sum_{s}\sum_{g}\frac{\Phi(\mathbf{g}|\mathbf{s})^{*}}{||\Phi(\mathbf{g}|\mathbf{s})||}\frac{\tilde{\Phi}(\mathbf{g}|\mathbf{s})}{||\tilde{\Phi}(\mathbf{g}|\mathbf{s})||}, \tag{2}$$

where the gradient in equation 2 with respect to the perturbation in slowness is

$$\frac{\partial \varepsilon}{\partial s(\mathbf{x})} = -\sum_{\omega}\sum_{s}\sum_{g}\frac{1}{||\Phi(\mathbf{g}|\mathbf{s})||}\frac{\partial \Phi}{\partial s(\mathbf{x})}[w\frac{\Phi(\mathbf{g}|\mathbf{s})}{||\Phi(\mathbf{g}|\mathbf{s})||} - \frac{\tilde{\Phi}(\mathbf{g}|\mathbf{s})}{||\tilde{\Phi}(\mathbf{g}|\mathbf{s})||}], \tag{3}$$

where w is the weight given by $w = \frac{\Phi(\mathbf{g}|\mathbf{s})}{||\Phi(\mathbf{g}|\mathbf{s})||}\cdot\frac{\tilde{\Phi}(\mathbf{g}|\mathbf{s})}{||\tilde{\Phi}(\mathbf{g}|\mathbf{s})||}$ which emphasizes the mismatch between the observed and the predicted crosscorrelograms. Substituting the expression for predicted crosscorrelograms in equation 1 into equation 3 gives

$$\frac{\partial \varepsilon}{\partial s(\mathbf{x})} = -\frac{\partial D^{*}(\mathbf{g}|\mathbf{s})}{\partial s(\mathbf{x})}\frac{1}{||\Phi(\mathbf{g}|\mathbf{s})||}D(\mathbf{g}|\mathbf{s})_{ref}[w\frac{\Phi(\mathbf{g}|\mathbf{s})}{||\Phi(\mathbf{g}|\mathbf{s})||} - \frac{\tilde{\Phi}(\mathbf{g}|\mathbf{s})}{||\tilde{\Phi}(\mathbf{g}|\mathbf{s})||}], \tag{4}$$

where the Frechét derivative $\frac{\partial D(\mathbf{g}|\mathbf{s})}{\partial s(\mathbf{x})}$ is given by Luo and Schuster (1991) as

$$\frac{\partial D(\mathbf{g}|\mathbf{s})}{\partial s(\mathbf{x})} = 2\omega^{2}s(\mathbf{x})G(\mathbf{g}|\mathbf{x})G(\mathbf{x}|\mathbf{s}). \tag{5}$$

Equation 4 says that the interferometric gradient (or migration image) is formed by smearing the weighted data residual along the associated migration ellipses. In the next section, we derive an interpretation of the gradient using the asymptotic Green's functions.

Interpretation of the ILSM gradient

The asymptotic high-frequency Green's function for a reflection from the subsurface point at $\mathbf{x_0}$ is defined as

$$D(\mathbf{g}|\mathbf{s}) = A(\mathbf{g},\mathbf{s})e^{i\omega(\tau_{\mathbf{sx_0}}+\tau_{\mathbf{gx_0}})}, \tag{6}$$

where $\tau_{\mathbf{sx_0}} + \tau_{\mathbf{gx_0}}$ is the traveltime from the source $\mathbf{s}$ to the receiver $\mathbf{g}$ for a reflection at point $\mathbf{x_0}$ in the subsurface, $A(\mathbf{g,s})$ is

DOI http://dx.doi.org/10.1190/segam2015-5858700.1

an amplitude term. Similarly, the Green's function for a reflection on the reference reflector, as shown in the Figure 1, can be defined as

$$D(\mathbf{g}|\mathbf{s})_{ref} = A'(\mathbf{g},\mathbf{s})e^{i\omega\tau_{\mathbf{sg}}{}^{ref}}, \tag{7}$$

where $\tau_{\mathbf{sg}}{}^{ref}$ is the calculated reflection time to the reference layer for a source at **s** and geophone at **g**. The predicted cross-

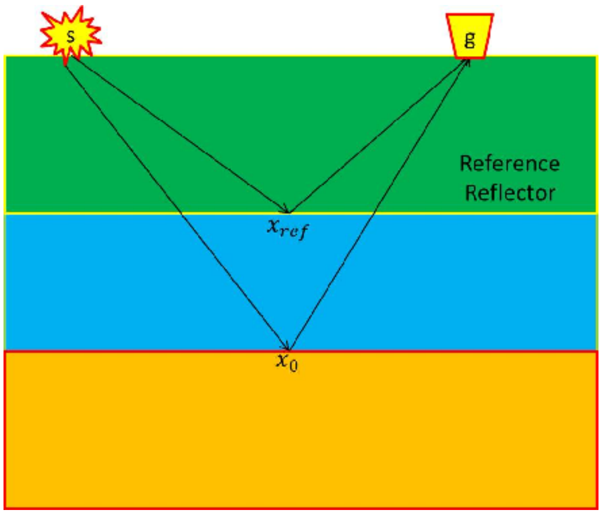

Figure 1: A crosscorrelogram is obtained by cross-correlating a recorded trace with the same trace windowed around the reference reflection.

correlogram $\Phi(\mathbf{g}|\mathbf{s})$ can be obtained by cross-correlating the predicted data with the picked reference reflection in the predicted data. The cross-correlation operation of the predicted data can be approximated by

$$\Phi(\mathbf{g}|\mathbf{s}) = D(\mathbf{g}|\mathbf{s})e^{-i\omega\tau_{\mathbf{sg}}{}^{ref}}. \tag{8}$$

Similarly, observed cross-correlogram $\tilde{\Phi}(\mathbf{g}|\mathbf{s})$ can be calculated as the

$$\tilde{\Phi}(\mathbf{g}|\mathbf{s}) = \tilde{D}(\mathbf{g}|\mathbf{s})e^{-i\omega\tilde{\tau}_{\mathbf{sg}}^{ref}}, \tag{9}$$

where $\tilde{\tau}_{\mathbf{sg}}$ is the picked reflection traveltime from the reference layer for a source at **s** and a geophone at **g**. Ignoring the normalization factor the weighted residual in equation 4 can be calculated as

$$\Delta\Phi(\mathbf{g}|\mathbf{s}) = w\Phi(\mathbf{g}|\mathbf{s}) - \tilde{\Phi}(\mathbf{g}|\mathbf{s}), \tag{10}$$

where w is the weight given by $w = \frac{\Phi(\mathbf{g}|\mathbf{s})}{||\Phi(\mathbf{g}|\mathbf{s})||} \cdot \frac{\tilde{\Phi}(\mathbf{g}|\mathbf{s})}{||\tilde{\Phi}(\mathbf{g}|\mathbf{s})||}$. Substituting the residual $\Delta\Phi(\mathbf{g}|\mathbf{s})$ and $D(\mathbf{g}|\mathbf{s})_{ref}$ from equation 7 into equation 4 we get the following expression for the gradient $\frac{\partial\varepsilon}{\partial s(\mathbf{x})}$

$$\frac{\partial\varepsilon}{\partial s(\mathbf{x})} = \sum_{\omega}\sum_{\mathbf{s}}\sum_{\mathbf{g}}\Delta\Phi(\mathbf{g}|\mathbf{s})e^{-i\omega(\tau_{\mathbf{sx}}+\tau_{\mathbf{xg}}-\tau_{\mathbf{sg}}{}^{\mathbf{ref}})}. \tag{11}$$

Amplitude term associated with $D(\mathbf{g}|\mathbf{s})_{ref}$ are conveniently ignored for this analysis. Substituting equations 8 and 9 in equation 10 we get

$$\Delta\Phi(\mathbf{g}|\mathbf{s}) = wD(\mathbf{g}|\mathbf{s})e^{-i\omega\tau_{\mathbf{sg}}{}^{ref}} - \tilde{D}(\mathbf{g}|\mathbf{s})e^{-i\omega\tilde{\tau}_{\mathbf{sg}}^{ref}}, \tag{12}$$

and using the expression for $\Delta\Phi(\mathbf{g}|\mathbf{s})$ in equation 12 we can further simplify equation 11 as

$$\frac{\partial\varepsilon}{\partial s(\mathbf{x})} = \sum_{\omega}\sum_{\mathbf{s}}\sum_{\mathbf{g}}[wD(\mathbf{g}|\mathbf{s}) - \tilde{D}(\mathbf{g}|\mathbf{s})e^{i\omega\overbrace{(\tau_{sg}{}^{ref} - \tilde{\tau}_{sg}^{ref})}^{\delta^{ref}\ timing\ error}}]\overbrace{e^{-i\omega(\tau_{\mathbf{sx}}+\tau_{\mathbf{xg}})}}^{migration\ kernel}.$$

The term δ^{ref} is the error in timing of the reference reflector due to statics. At each step of ILSM the gradient is calculated by migrating the data residual, which is calculated by temporally shifting the observed trace by δ^{ref} and then subtracting it from the weighted predicted trace $wD(\mathbf{g}|\mathbf{s})$. Shifting the observed trace by δ^{ref} is similar to applying a statics correction to the data. The next subsection describes the workflow of the method.

Workflow

- Define a reference reflector in the reflectivity model and window the corresponding reference reflection in the observed data.
- Cross-correlate the observed data with observed reference reflection data to get the observed crosscorrelogram and calculate the interferometric residual as shown in equation 4.
- Calculate the gradient $\mathbf{g}^{k+1}$ shown in the equation 4 and update the search direction $\mathbf{d}^k$ using conjugate gradient (Nocedal and Wright (2006))

  $$\mathbf{d}^{k+1} = -\mathbf{g}^{k+1} + \beta\mathbf{d}^k, \tag{13}$$

  where β can be calculated using the Fletcher-Reeves formula.

  $$\beta = \frac{(\mathbf{g}^{k+1}, \mathbf{g}^{k+1})}{(\mathbf{g}^k, \mathbf{g}^k)}. \tag{14}$$

- Compute the step length α by

  $$\alpha = \frac{(\mathbf{d}^{k+1}, \mathbf{g}^{k+1})}{(\mathbf{L}\mathbf{d}^{k+1}, \mathbf{L}\mathbf{d}^{k+1})}. \tag{15}$$

- Update the migration image m^{k+1} by

  $$\mathbf{m}^{k+1} = \mathbf{m}^k + \alpha\mathbf{d}^{k+1}. \tag{16}$$

- Calculate the new predicted crosscorrelogram using equation 1.

The effectiveness of ILSM in mitigating statics at the near surface is now illustrated with numerical examples.

NUMERICAL EXAMPLES

ILSM is tested on a fault model derived from a 2-D section of the 3D SEG-EAGE salt model with several low-velocity anomalies introduced in the near-surface region. Figure 2 depicts the true velocity model used to generate the observed data and the migration velocity model. The reflectivity model used for generating the data is shown in Figure 3, and the curved reflector on the top is chosen as the reference reflector. Kirchoff-Born modeling was used to generate synthetic

DOI http://dx.doi.org/10.1190/segam2015-5858700.1

data. A fixed-spread acquisition is used with 50 shots sampled every 50 m on the surface. Each shot is recorded with 501 receivers spaced every 5 m on the surface with a recording time of 4 seconds. Kirchoff migration is used for both least-squares migration (LSM) and ILSM in imaging these data. The conventional LSM and ILSM images obtained after 20 iterations are shown in Figure 4. The reflectors in the ILSM image are better focused compared to the LSM image. The deeper reflectors are a bit distorted because the timing error of the reference reflection does not account for a perfect static correction for the later reflections. But the defocusing due to the static errors is reduced and a better migration image is inverted. ILSM is also tested on a Gulf of Mexico (GoM) dataset. The data consists of 515 shot gathers with a shot interval of 37.5 m. There are 480 receivers in each shot gather with receivers placed every 12.5 m along a line. To replicate a scenario where data contain statics , low-velocity errors are incorporated to the original tomogram. The original tomogram inverted by Huang (2013) is shown in Figure 5(a) and the LSM image obtained after 10 iterations using this velocity model is shown in Figure 6(a). The sea-bottom reflector is chosen as the reference reflector for ILSM. Errors are added to the original tomogram and the resulting erroneous velocity model is shown in Figure 5(b). The LSM and ILSM images obtained after 10 iterations using this velocity model are shown in Figures 6(b) and 6(c) respectively. The zoom views of the dashed orange and yellow boxes are shown in Figure 7. LSM is not able to image accurately because of errors in the velocity model. ILSM is able to image

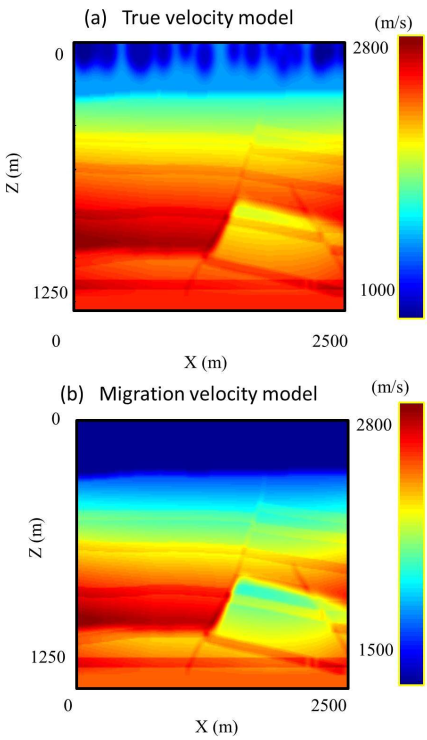

Figure 2: (a) Velocity model used for generating the observed data. (b) Velocity model used for ILSM and LSM.

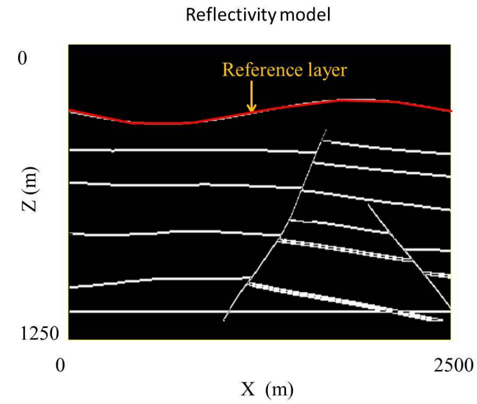

Figure 3: Reflectivity model used for generating data, where the curved reflector (in red) on the top is chosen as the reference layer.

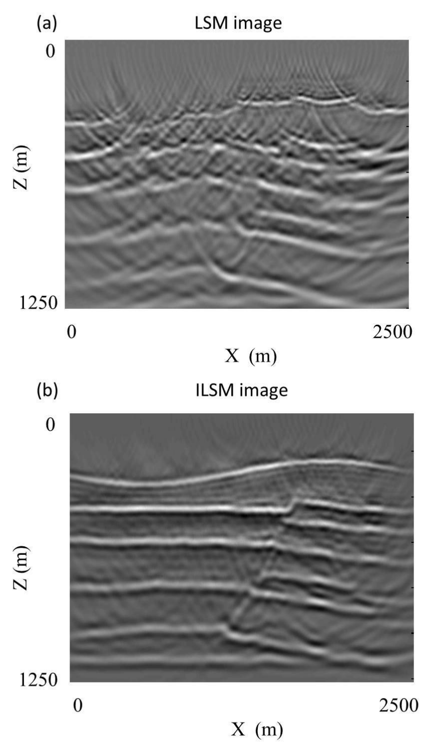

Figure 4: Migration images from (a) standard LSM and (b) ILSM.

DOI http://dx.doi.org/10.1190/segam2015-5858700.1

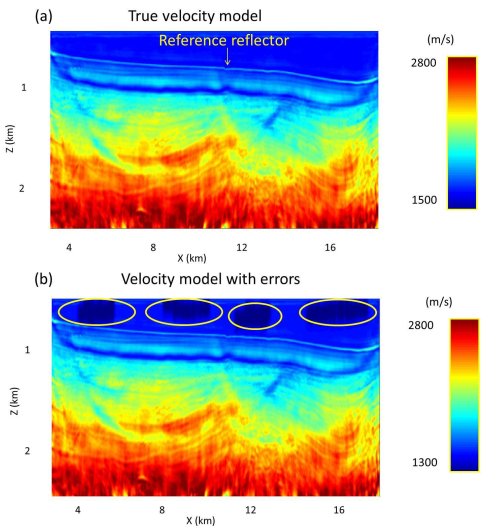

Figure 5: (a) Original velocity model and (b) velocity model with errors. The encircled areas indicate the regions in which the errors are added. The sea-bottom is chosen as the reference reflector.

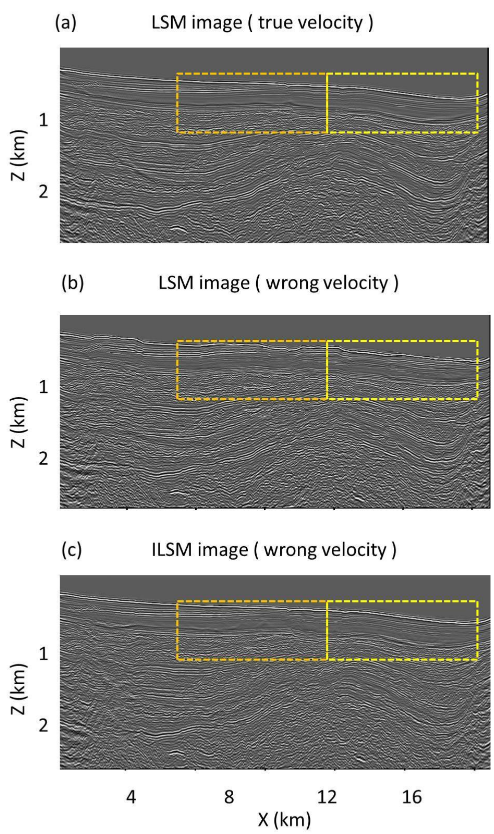

Figure 6: (a) LSM image from true velocity model, the sea-bottom is chosen as the reference reflector. (b) LSM image with erroneous velocity model. (c) ILSM image using erroneous velocity model.

the shallow reflectors accurately owing to the fact that these reflectors lie in close proximity to the sea-bottom reflector, on the other hand the deeper reflectors located far away from the sea-bottom reflector are not imaged accurately.

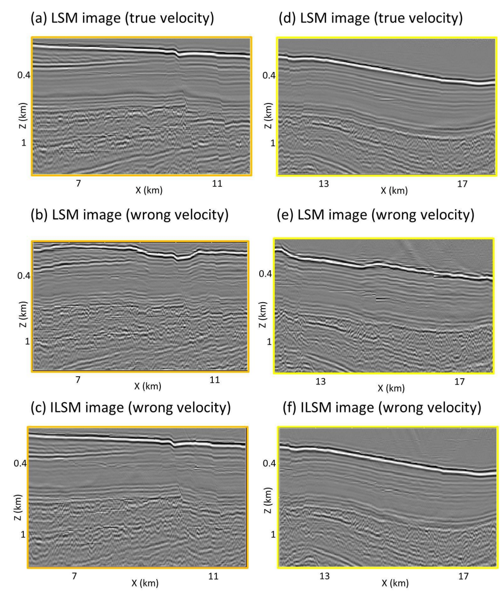

Figure 7: Zoom views of dashed boxes in Figure 6. (a) LSM image (orange box) using true velocity model. (b) LSM image (orange box) using erroneous velocity model. (c) ILSM image (orange box) using erroneous velocity model. (d) LSM image (yellow box) using true velocity model. (e) LSM image (yellow box) using erroneous velocity model. (f) ILSM image (yellow box) using erroneous velocity model.

CONCLUSIONS

ILSM has the potential to mitigate source and receiver statics. A reference reflector must be identified and each trace is windowed around the reference reflection and then crosscorrelated with the trace. These weighted crosscorrelograms are iteratively migrated to estimate the migration image of the subsurface. Preliminary numerical tests show that ILSM can mitigate the defocusing in migration images because of statics. However, reflectors located far away from the reference reflector do not get imaged accurately. This problem can be partly alleviated by iteratively identifying deeper reference reflectors and using them to image just below them.

ACKNOWLEDGMENTS

We thank the sponsors of the CSIM consortium for their support. I would also like to thank the high performance computing (HPC) center of KAUST for providing access to supercomputing facilities .

DOI http://dx.doi.org/10.1190/segam2015-5858700.1

EDITED REFERENCES
Note: This reference list is a copyedited version of the reference list submitted by the author. Reference lists for the 2015 SEG Technical Program Expanded Abstracts have been copyedited so that references provided with the online metadata for each paper will achieve a high degree of linking to cited sources that appear on the Web.

REFERENCES

Dutta, G., M. Sinha, and G. T. Schuster, 2014, A crosscorrelation objective function for least-squares migration and visco-acoustic imaging: 84th Annual International Meeting, SEG, Expanded Abstracts, 3985–3990, doi: 10.1190/segam2014-1376.1.

Huang, Y., 2013, Least-squares migration and full waveform inversion with multisource frequency selection: Ph.D. thesis, King Abdullah University of Science and Technology.

Luo, Y., and G. T. Schuster, 1991, Wave equation travel time inversion: Geophysics, **56**, 645–653. http://dx.doi.org/10.1190/1.1443081.

Nocedal, J., and S. Wright, 2006, Numerical optimization: Springer.

Routh, P., J. Krebs, S. Lazaratos, A. Baumstein, I. Chikichev, S. Lee, N. Downey, D. Hinkley, and J. Anderson, 2011, Full-wavefield inversion of marine streamer data with the encoded simultaneous source method: 73rd Annual International Conference and Exhibition, Extended Abstracts, EAGE, F032.

Zhang, Y., L. Duan, and Y. Xie, 2013, A stable and practical implementation of least-squares reverse time migration: 83rd Annual International Meeting, Expanded Abstracts, SEG, 3716–3720, doi: 10.1190/segam2013-0577.1.

Zhou, M., Z. Jiang, J. Yu, and G. T. Schuster, 2006, Comparison between interferometric migration and reduced-time migration of common-depth-point data: Geophysics, **71**, no. 4, SI189–SI196. http://dx.doi.org/10.1190/1.2213046.